Numerical Simulation of Emission Spectra from Ion Beam-Heated Aluminum Plasmas

J.J. MacFarlane, P. Wang

January 1991

UWFDM-848

Lasers & Part. Beams 10 (1992) 349.

FUSION TECHNOLOGY INSTITUTE

UNIVERSITY OF WISCONSIN

MADISON WISCONSIN

Numerical Simulation of Emission Spectra from Ion Beam-Heated Aluminum Plasmas

J.J. MacFarlane, P. Wang

Fusion Technology Institute
University of Wisconsin
1500 Engineering Drive
Madison, WI 53706

http://fti.neep.wisc.edu

January 1991

UWFDM-848

Lasers & Part. Beams 10 (1992) 349.

Numerical Simulation of Emission Spectra from Ion Beam-Heated Aluminum Plasmas

J.J. MacFarlane and P. Wang

Fusion Technology Institute
Nuclear Engineering and Engineering Physics Department
University of Wisconsin-Madison
1500 Johnson Drive
Madison WI 53706

February 1991

UWFDM-848

Submitted to Lasers and Particle Beams.

Abstract

Non-LTE radiative transfer calculations have been performed to predict emission spectra from plasmas heated by intense proton beams. Multilevel, steady-state atomic rate equations were solved self-consistently with the radiation field to determine excitation and ionization populations. Ion beam effects were included in the rate equations. Proton-impact ionization cross sections were calculated using a plane wave Born approximation model with Hartree-Fock wave functions for the electrons. We have examined the dependence of emission spectra on the temperature and thickness of the plasma. In addition, K_α satellite line spectra were computed to assess its potential as a temperature diagnostic. Calculated K_α spectral results are compared with recent PBFA II experimental data.

1. Introduction

The study of high energy density plasmas created by intense ion beams has received an increasing amount of attention in recent years. Pulsed power accelerators, such as PBFA II (Particle Beam Fusion Accelerator II) at Sandia National Laboratories and KALIF (the Karlsruhe Light Ion Facility) at Kernforschungszentrum Karlsruhe, can generate high intensity, multi-MeV proton beams (Bailey *et al.* 1990; Bauer, Bluhm, and Goel 1988). Also, high intensity heavy ion beams are used to create high temperature plasmas at Gesellschaft für Schwerionenforschung (GSI) in Darmstadt (Meyer-ter-Vehn and Witkowski 1990; Hoffmann, Hofmann, and Meyer-ter-Vehn 1990). Experiments carried out at these facilities will lead to an improved understanding of the physics of high energy density plasmas and beam-plasma interactions, areas of vital concern to ion-driven inertial confinement fusion (ICF).

Plasma conditions obtained in beam-plasma interaction experiments can be deduced from radiation spectra. Theoretical analysis of such spectra is often complicated by the fact that the plasmas are often *not* in local thermodynamic equilibrium (LTE). That is, the excitation and ionization populations cannot be reliably approximated by Boltzmann statistics and the Saha equation (see, *e.g.*, MacFarlane, Wang, and Moses 1990a, 1990b; Rogerson, Clark, and Davis 1985). This is because both the radiation field and ion beam can drive the populations out of LTE. Reliable theoretical analysis of such spectra often requires detailed models which include the effects of the radiation field and ion beam.

The purpose of this paper is to show how emission spectra from ion beam-heated plasmas are affected by plasma conditions, and to examine which parts of the spectrum present good opportunities for diagnosing plasma conditions. In particular, we have calculated the spectral flux from Al plasmas with temperatures $\sim$ 5 eV to 50 eV and ion densities $\sim 10^{-2}$ to 10^{-1} n_0 ($n_0 \equiv$ solid density) to study how the spectrum is influenced by the temperature and size of the plasma. We have also calculated K_α spectral line fluxes. These soft x-ray lines are byproducts of proton-impact ionization of K-shell electrons. In these preliminary calculations, we have studied the dependence of the K_α spectrum on temperature, as well as the influence of line self-attenuation on the emergent flux. Calculated K_α spectra are compared with experimental data recently obtained in proton beam experiments on PBFA II (Bailey *et al.* 1990). It is shown that the K_α spectral region has considerable potential for diagnosing plasma conditions in beam-plasma interaction experiments.

2. Theoretical Models

In this section, we present a brief overview of the theoretical models used to compute the emission spectra from beam-heated plasmas. A detailed description of these models is

presented elsewhere (MacFarlane, Wang, and Moses 1990a, 1990b; MacFarlane, Wang, and Henderson 1991; Wang 1991).

2.1. Overview of Radiative Transfer/Ionization Balance Model

Steady-state ionization and excitation populations are computed by solving multilevel atomic rate equations self-consistently with the radiation field. This is a collisional-radiative equilibrium (CRE) model which includes the effects of photoexcitation and photoionization on the level populations. Detailed configuration accounting (DCA) is used to track the populations of the atomic levels. Thus, the population of each atomic level is determined by computing the collisional and radiative transition rates between each level. This type of model — as opposed to an average atom model, for instance — must be used to compute the detailed radiation spectra from laboratory plasmas.

In our calculations for Al plasmas, we consider a total of 105 energy levels distributed over all 14 ionization stages. Of these, 27 are autoionizing levels which represent the initial states in K_α fluorescence transitions. The ionization processes considered in determining the atomic level populations are collisional ionization and recombination, photoionization and stimulated recombination, and radiative and dielectronic recombination. Except for dielectronic recombination, every state of an ion is coupled to the ground state of the next higher ionization stage by each ionization/recombination process. Only the ground states of adjacent ions are coupled for dielectronic recombination. In problems where proton beam effects are important (such as when computing the K_α line spectrum), proton-impact ionization and autoionization rates are also included. All of the autoionizing levels are coupled to the next lower ionization stage by proton-impact ionization, and the next higher ionization stage by autoionization. The excitation processes considered are collisional excitation and deexcitation, photoexcitation and stimulated emission, and spontaneous radiative decay. A schematic illustration of the transitions considered in our model (excluding proton-impact ionization and autoionizing transitions) is shown in Figure 1 for the case of a simple 3-level atom.

The photoexcitation and photoionization rates depend on the characteristics of the radiation field. To evaluate these rates we use an escape probability radiation transport model (Apruzese *et al.* 1980; Apruzese 1981; MacFarlane *et al.* 1990a, 1990b). This model employs angle- and frequency-averaging techniques that allow for computationally efficient solutions that produce only a modest loss in accuracy. The motivation for using this approach for non-LTE radiative transfer is that it can be coupled with hydrodynamics codes to study rapidly changing laboratory plasmas (Duston *et al.* 1983; Apruzese *et al.* 1984; Clark *et al.* 1986).

To model the effects of collisional line broadening, lines are assumed to have Voigt

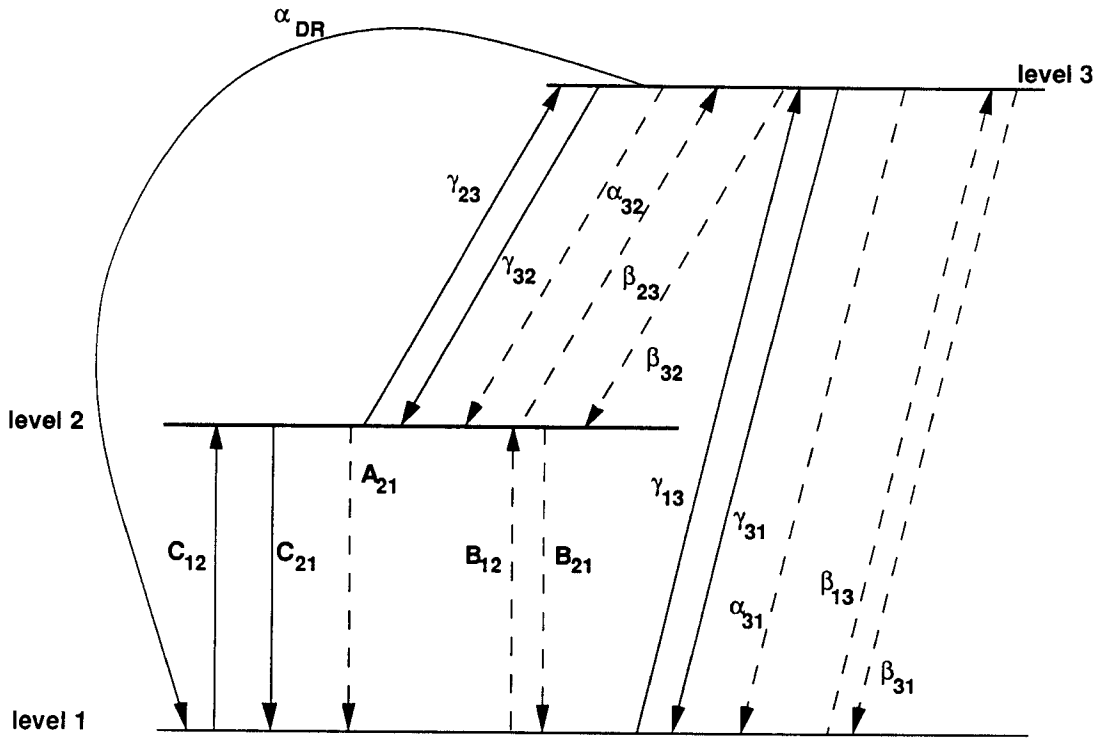

C_{ij} → collisional excitation ($i < j$) or deexcitation ($i > j$)

A_{ij} → spontaneous emission

B_{ij} → photoexcitation ($i < j$) or stimulated emission ($i > j$)

γ_{ij} → collisional ionization ($i < j$) or recombination ($i > j$)

α_{ij} → radiative recombination

α_{DR} → dielectronic recombination

β_{ij} → photoionization ($i < j$) or stimulated recombination ($i > j$)

Figure 1. Schematic illustration of the transitions in a 3-level atom.

profiles with the damping parameter for each transition ($u \rightarrow \ell$) given by (Duston and Davis 1981):

$$a_{u\ell} = \frac{\Gamma_{u\ell}}{4\pi\Delta\nu_D}, \tag{1}$$

where $\Delta\nu_D$ is the Doppler width, and $\Gamma_{u\ell}$ represents the sum of all radiative and collisional rates, R_{ij} and C_{ij}, depopulating the upper and lower levels:

$$\Gamma_{u\ell} = \sum_k (C_{uk} + R_{uk}) + \sum_k (C_{\ell k} + R_{\ell k}). \tag{2}$$

Bound-bound, bound-free, and free-free contributions to the emissivity and opacity are considered in computing frequency-dependent emission spectra.

2.2. Atomic Physics Models

Rate coefficients for the ionization and excitation processes not involving proton-impact ionization and autoionization are described elsewhere (MacFarlane *et al.* 1990b; Wang 1991), and only a brief summary will be given here. We perform Hartree-Fock calculations to determine energy levels, oscillator strengths, and photoionization and radiative recombination rates. The interaction between bound electrons is approximated by an $L-S$ coupling scheme. Collisional excitation and deexcitation rates and collisional ionization and recombination rates are calculated using a combination of semiclassical impact parameter, Born-Oppenheimer, and distorted wave models (Burgess and Summer 1976; Solbelman, Vainshtein, and Yukov 1981). Dielectronic recombination rates are computed using the Burgess-Mertz model (Post *et al.* 1977) in conjunction with Hartree-Fock energies and oscillator strengths.

For problems involving ion beam-plasma interactions, we also consider the effects of ion-impact ionization and autoionization. Autoionization rates are determined from the spontaneous emission rates and the fluorescence yield of each Al ion (Duston *et al.* 1983). The calculations of the proton-impact ionization cross sections are based on the plane-wave Born approximation (Merzbacher and Lewis 1958). Hartree-Fock wave functions are used for the electrons.

Figure 2 shows the calculated cross sections for each shell of neutral Al as a function of incident proton energy. Note that the outer shell cross sections are substantially larger that the inner shell values. Thus, the primary *heating* (*i.e.*, ion stopping) mechanism is the interaction of the proton beam with the outer shell electrons. Although K-shell ionization

is not important to the heating of the plasma, it can play an important role in diagnosing plasma conditions. Also in Figure 2, the calculated cross sections for the *1s* shell are compared with experimental data (Khan, Potter, and Worley 1965). For proton energies $\sim$ 0.1 MeV to 1.0 MeV, our calculated cross sections are seen to be accurate to within a factor of 2. It is expected that the accuracy of the calculations will become even better at higher proton energies as the assumptions in the PWBA model become more reliable.

Figure 3 shows how the proton-impact ionization cross section for Al K-shell electrons varies with the ionization stage of Al. As the ionization stage of the Al increases the cross section decreases in an almost linear fashion. Our calculations indicate that the proton-impact ionization cross section for the K-shell electrons for Al II is about a factor of 2 higher than that for Al XIII.

To determine the wavelengths of term-dependent K_α satellite lines accurately, we have calculated the energies of the levels involved in K_α transitions using a multiconfiguration Hartree-Fock model (Froese Fischer 1978) with relativistic mass and Darwin corrections. These calculations for states which have vacancies in the *1s* shell represent a significant improvement over nonrelativistic single-configuration Hartree-Fock calculations. Accurate wavelengths allow one to more confidently determine the transitions which are responsible for the peaks in experimental spectra. This is of course very desirable for diagnosing plasma conditions. A detailed description of these calculations will be published in a future paper.

3. Results

We have performed a series of calculations to predict the emission spectra from targets in beam-plasma interaction experiments. The purpose of the calculations is to develop an understanding of the physical processes that influence the emission spectra from targets, and to identify spectral features that can be used to deduce plasma conditions. The calculations presented here are for Al plasmas with temperatures in the 5 to 50 eV range and densities of $10^{-2} - 10^{-1}$ times solid density. All calculations presented in this section are for planar plasmas with uniform temperatures and densities. We first discuss the general features of target emission spectra. In particular, we will show how the overall spectrum changes as a function of slab thickness and temperature. We then examine the potential for using K_α satellite lines as a temperature diagnostic for ion beam-heated plasmas. These lines, which result from ion-impact ionization of target ions by the incoming beams, can be seen in the soft x-ray part of the spectrum (near 1.5 keV for Al).

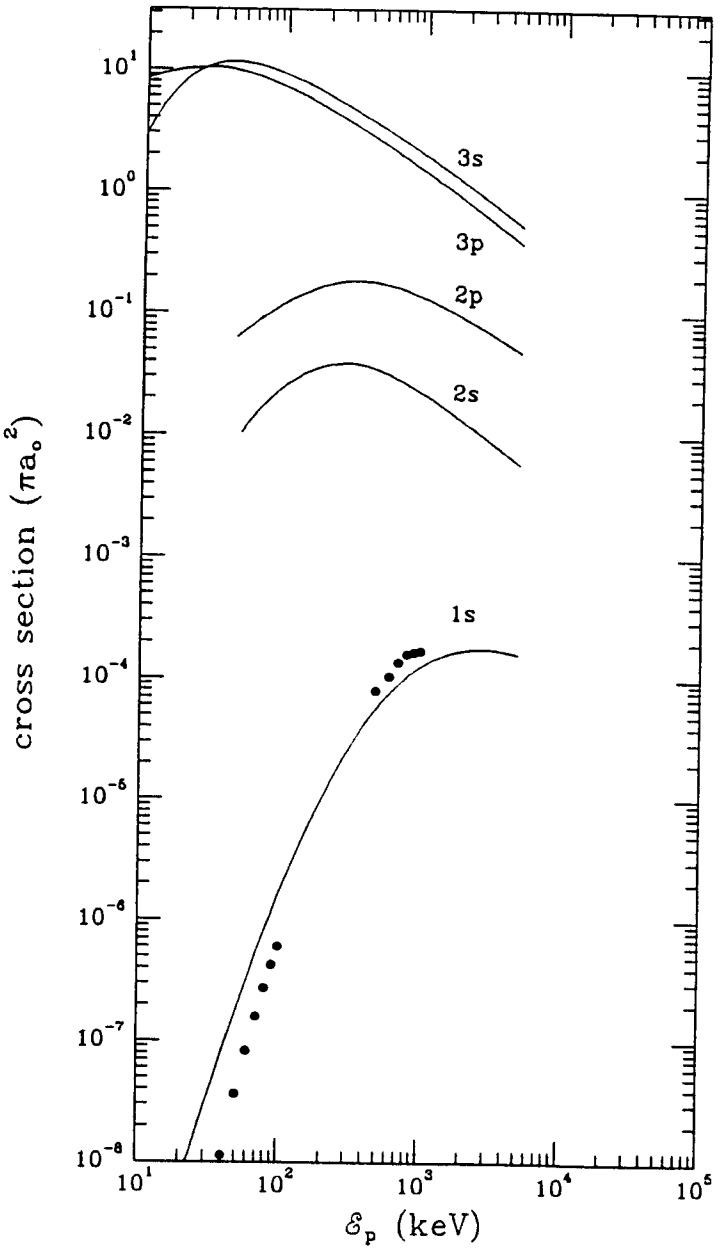

Figure 2. Proton-impact ionization cross sections for all shells of neutral Al. The circles represent the experimental data of Kahn, Potter, and Worley (1965).

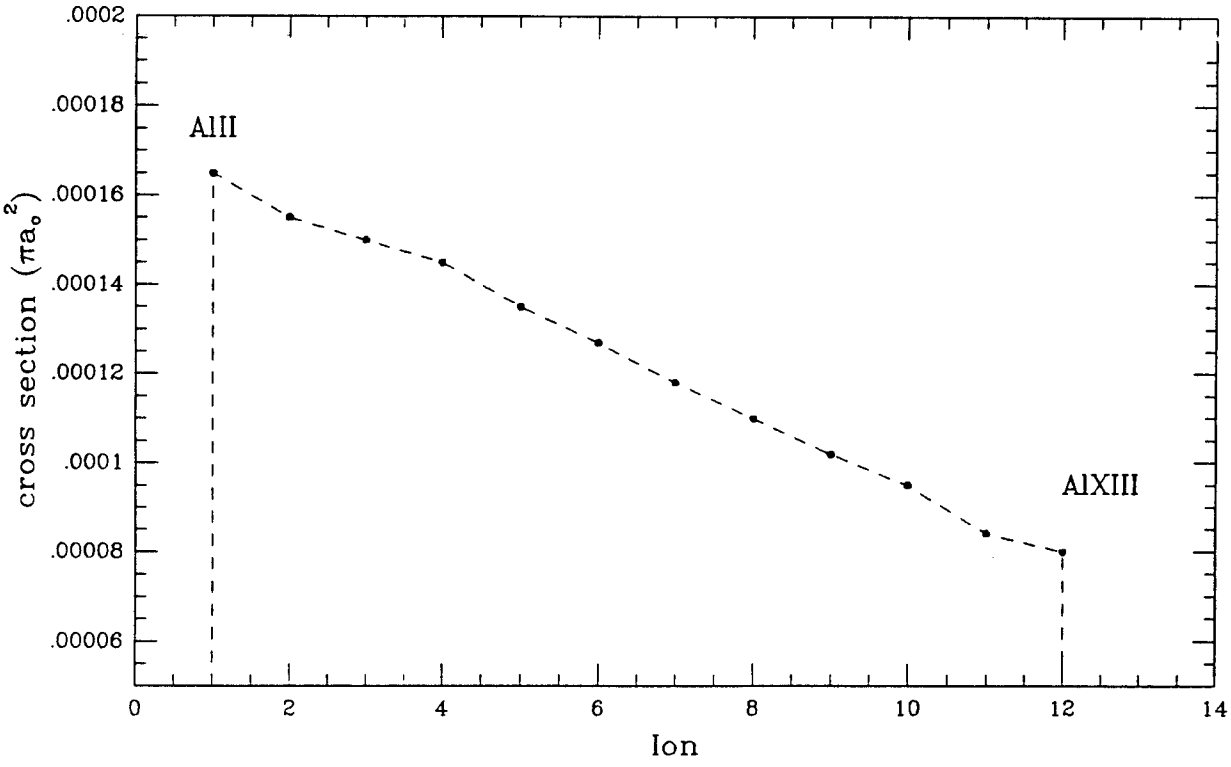

Figure 3. Dependence of the proton-impact ionization cross section for K-shell electrons on the ionization stage of Al. The energy of the incident proton is 5 MeV.

3.1. Emission Spectra of Moderately-Ionized Aluminum

We first examine the emission spectra from Al targets in the absence of an ion beam; *i.e.*, with no proton-impact ionization and K_α line emission. We consider the case of a planar Al foil which has expanded 100 times from its original thickness L_0. Assuming the plasma has a uniform density of $n = 10^{-2}\ n_0$ ($n_0 = 6 \times 10^{22}$ cm^{-3} for Al) and temperature T, we examine how the spectral flux varies with original foil thickness and temperature.

Figure 4 shows the spectral fluxes for Al plasmas corresponding to an *original* foil thickness of 0.1, 1.0, and 10 μm, respectively. The thicknesses of the expanded plasma slabs are therefore 10^{-2}, 10^{-1}, and 1 mm. In each case, the plasma temperature is 50 eV and the density $10^{-2}\ n_0$. The blackbody flux is shown for comparison. Note that for clarity the fluxes for the 0.1 mm and 1.0 mm cases have been multiplied by 10^2 and 10^4, respectively. With an original foil thickness of 0.1 μm (bottom curve), the flux below photon energies of $h\nu \lesssim 10$ eV is basically blackbody. However, above 10 eV considerable structure is seen in the spectrum in the form of emission lines and bound-free edges. As the thickness of the foil increases, the flux becomes more like a blackbody over a wider spectral range. The top curve shows that for an Al foil with $L_0 = 10$ μm, the spectrum is very much like a blackbody.

The reason for dependence of the emission spectrum on the foil thickness can be understood by examining the frequency-dependence of the optical depth. Figure 5 shows the optical depths corresponding to the 1.0 mm and 0.01 mm cases. The optical depths correspond to the entire slab thickness and were computed along a ray perpendicular to the slab boundary. Note that when the original foil thickness is $\gtrsim 10$ μm (top curve), the plasma is optically thick ($\tau > 1$) at all photon energies below 1 keV. However, when $L_0 = 0.1$ μm (bottom curve), the plasma is optically thin to continuum radiation at photon energies above 10 eV. Only the line cores are optically thick at these higher frequencies. When the continuum is optically thin, emission lines become discernible in the spectrum.

The variation in the target emission spectrum with temperature is shown in Figure 6, where the spectral fluxes from Al plasmas with $T = 50$ eV, 15 eV, and 5 eV are shown. In each case, the plasma density is $n = 10^{-2}\ n_0$, $L = 10^{-2} L_0$, and $L_0 = 1.0$ μm. As the temperature rises from 5 eV to 50 eV, more structure can be observed in the emission spectrum. This is because at lower temperatures, the peak of the flux curve shifts to lower photon energies where the plasma tends to be optically thick.

Based on these results, the bulk of the radiation emitted by plasmas created during beam-plasma interaction experiments should have spectral fluxes which tend to resemble blackbody curves. This is because foil thicknesses, which are often constrained by the energy deposition properties of the beam, are typically $\gtrsim 10$ μm. This means that the plasma will be optically thick at most photon energies below 1 keV. When this occurs, it becomes

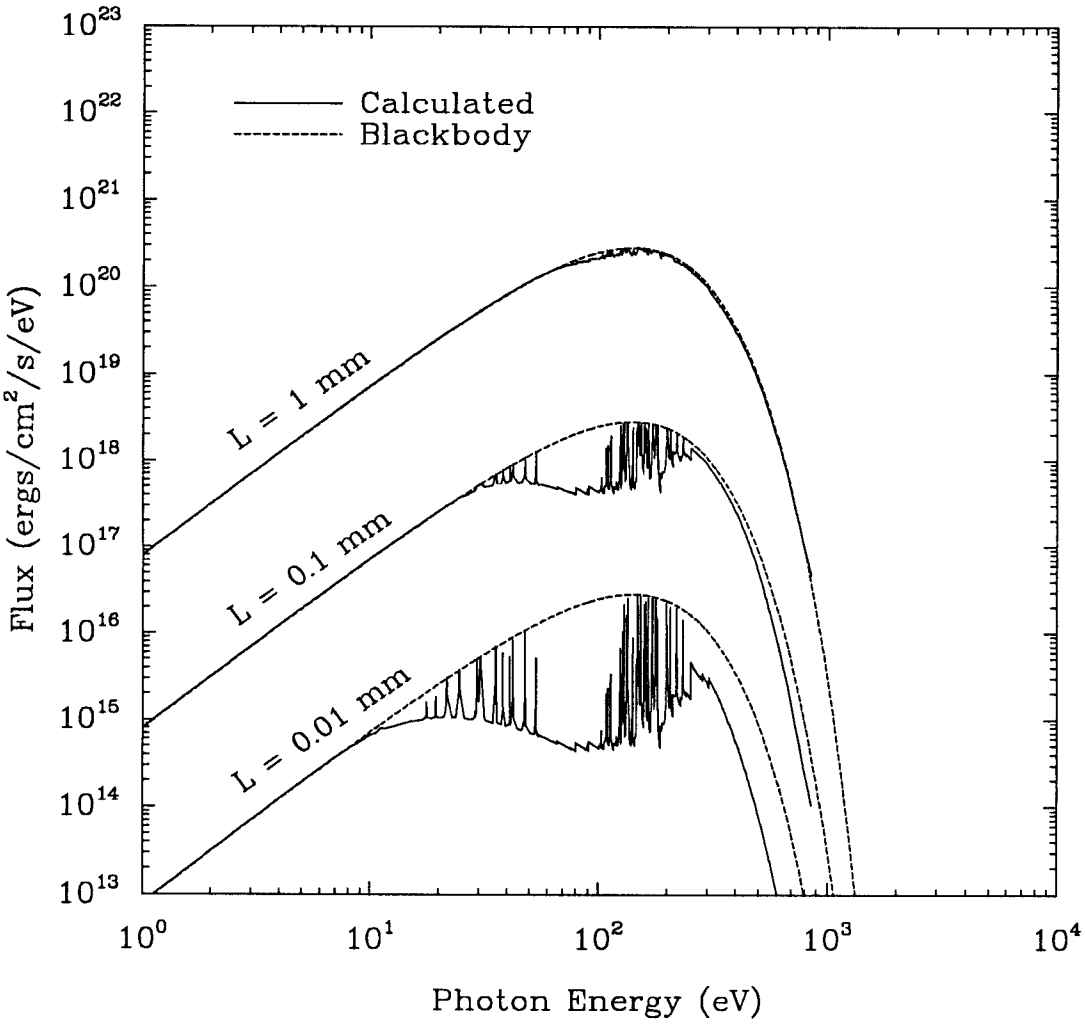

Figure 4. Dependence from the spectral flux on slab thickness for an Al plasma at $T =$ 50 eV and $n = 10^{-2}\ n_0$. The fluxes for the 0.1 mm and 1 mm cases have been multiplied by 10^2 and 10^4, respectively. The dashed curves represent the blackbody flux at $T = 50$ eV.

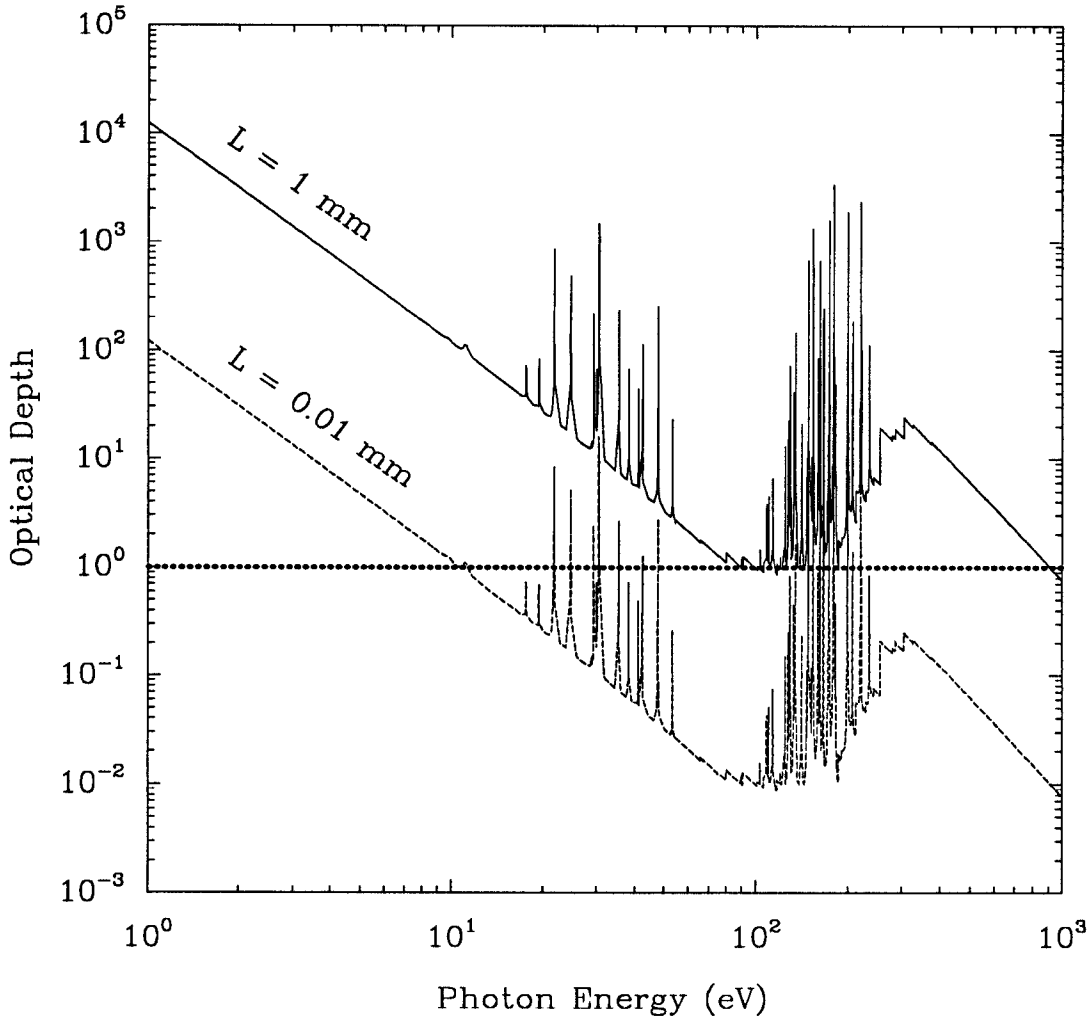

Figure 5. Dependence of optical depth on photon energy for the 0.01 mm and 1 mm cases shown in Figure 4. The dashed line at $\tau = 1$ represents the separation between the "optically thick" and "optically thin" regions.

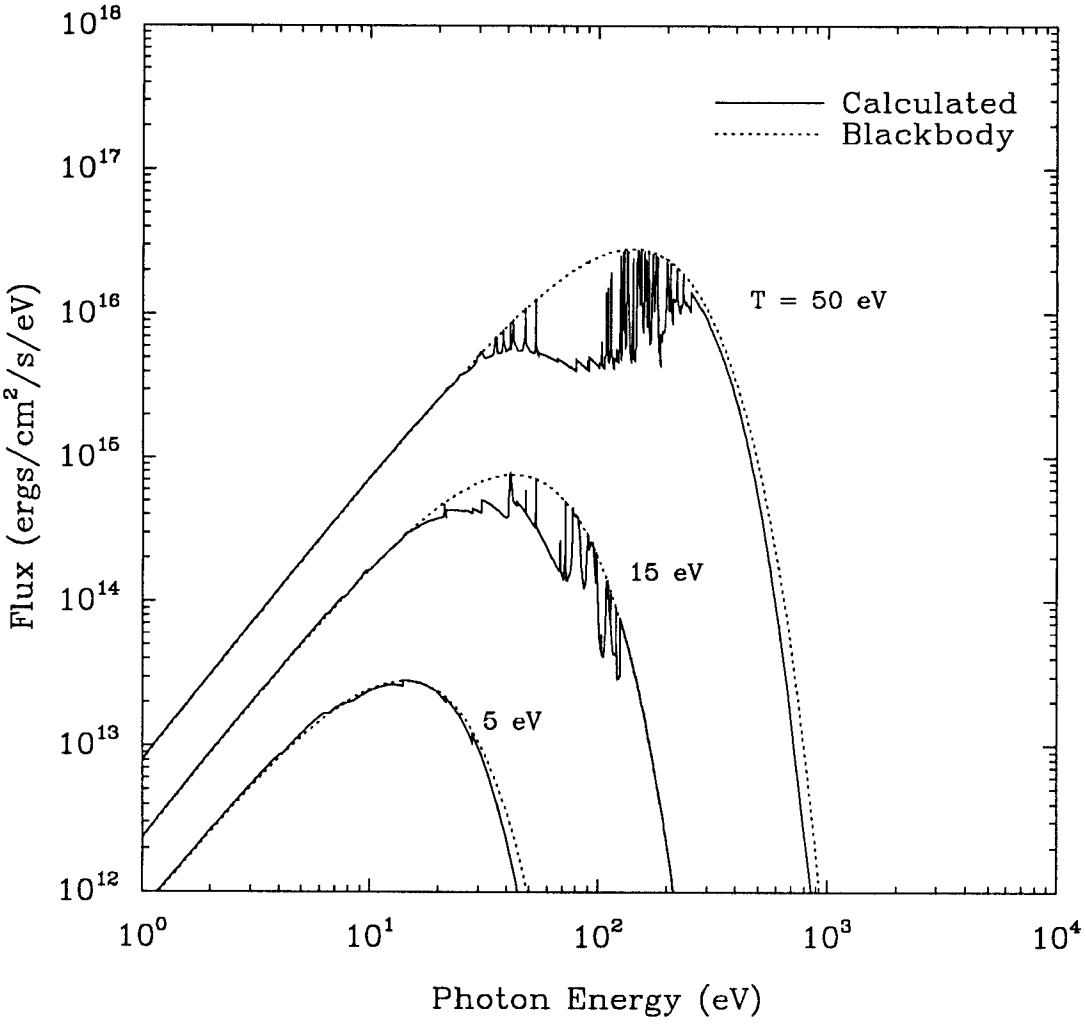

Figure 6. Spectral flux emitted from an Al plasma at $T = 5$ eV, 15 eV, and 50 eV. In each case, the slab thickness was 0.1 mm and $n = 10^{-2}\ n_0$. The dashed curves represent the blackbody flux for each temperature.

difficult for the detector to see into the interior of the plasma. We shall now focus on how radiation emitted in the soft x-ray portion of the spectrum for ion beam-heated plasmas can be used to diagnose plasma conditions.

3.2. K_α Satellite Line Spectra

Plasmas heated by intense ion or electron beams can emit detectable x-ray line radiation that can provide important constraints for diagnosing plasma conditions (Nardi and Zinamon 1981, Chenais-Popovics *et al.* 1989, Bailey *et al.* 1990). The reason is because energetic beams eject inner shell electrons of the target plasma, which can produce fluorescent line radiation as the inner shell vacancy is filled by an outer shell electron. Such lines are called K_α lines when a vacancy in the K-shell is filled with an electron from the L-shell. The production of K_α lines when a moderately-ionized Al plasma is irradiated by an intense proton beam is illustrated in Figure 7. For a plasma that is hot enough to have a significant amount of Al V, small concentrations of highly-excited Al VI are produced as a K-shell electron is ejected by proton-impact ionization. These highly-excited "autoionizing" levels are depopulated primarily in two ways: (1) a radiationless autoionization in which a second electron is ejected as the K-shell vacancy is filled, or (2) a spontaneous decay to a lower lying level of Al VI in which a photon with an energy of about 1.5 keV is emitted. Thus, a relatively cool plasma is capable of emitting soft x-ray lines because of the beam-plasma interaction. The wavelengths of the K_α lines become slightly blue-shifted as the ionization stage increases. The relative strengths of the K_α lines can be used to determine the ionization distribution in the plasma.

Figure 8 shows the spectral flux for an Al plasma which is being heated by a 1.6 MeV, 0.3 TW/cm^2 proton beam. The Al plasma is assumed to be at $T = 20$ eV, $n = 10^{-2}$ n_0, and $L = 1$ mm. This corresponds to an original foil thickness of 10 μm. Note that at photon energies below 0.5 keV the flux very much resembles a blackbody, a result of the plasma being optically thick at these photon energies. Near 1.5 keV, the K_α emission lines are clearly seen. Figure 9 shows the frequency-dependent optical depth for the same calculation. Clearly, the K_α lines can be optically thick, with optical depths exceeding 10^3. This indicates that the self-attenuation of line radiation will significantly affect the emission spectrum.

We now examine in detail the narrow region of the spectrum near 1.5 keV in which the K_α lines are located. Figure 10 shows the K_α line spectrum calculated for an Al plasma with a temperature of 10 eV, a density of 10^{-1} n_0, and original foil thickness of 10 μm. In this case, the proton beam energy and power density were 5 MeV and 5 TW/cm^2, respectively. For comparison, the *time-integrated* experimental spectrum obtained on PBFA II at Sandia National Laboratories is shown (Bailey *et al.* 1990). Note that two curves are shown in the experimental plot. The upper curve represents the lower curve values magnified 15 times.

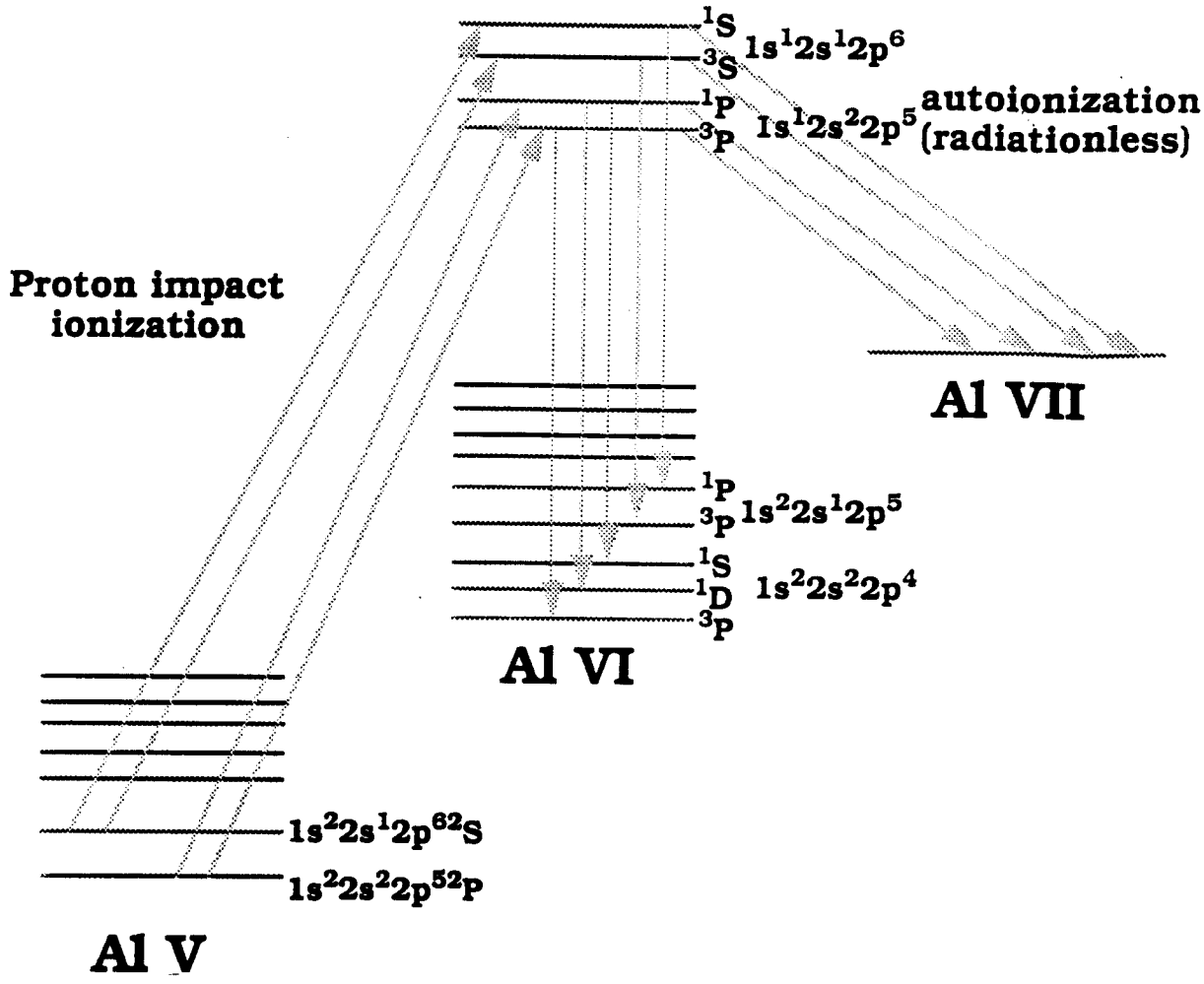

Figure 7. Schematic illustration of the atomic processes involved in the production of K_α fluorescence lines.

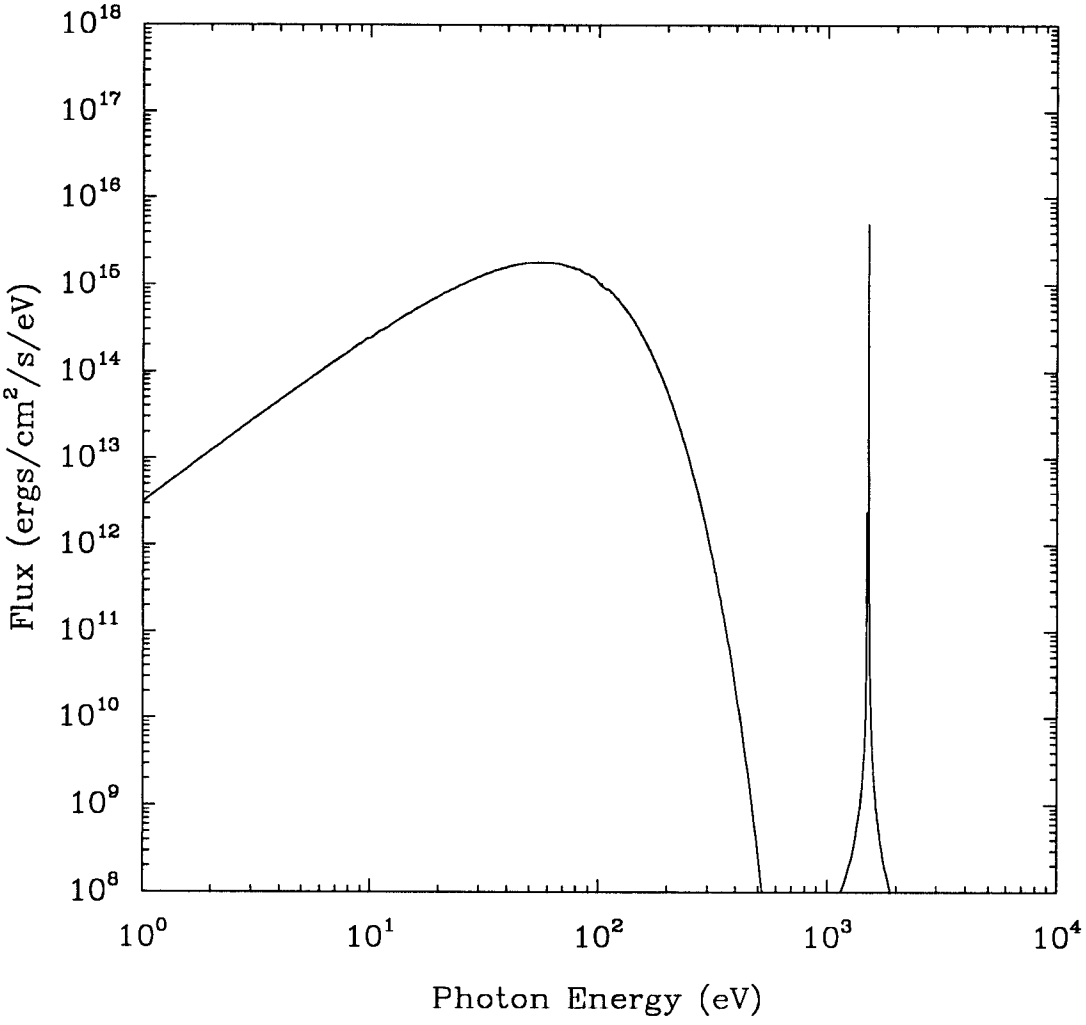

Figure 8. Spectral flux from an Al plasma being heated by a 1.6 MeV, 0.3 TW/cm^2 proton beam. The plasma conditions are $T = 20$ eV, $n = 10^{-2}\ n_0$, and $L = 1$ mm. The K_α lines are near 1.5 keV.

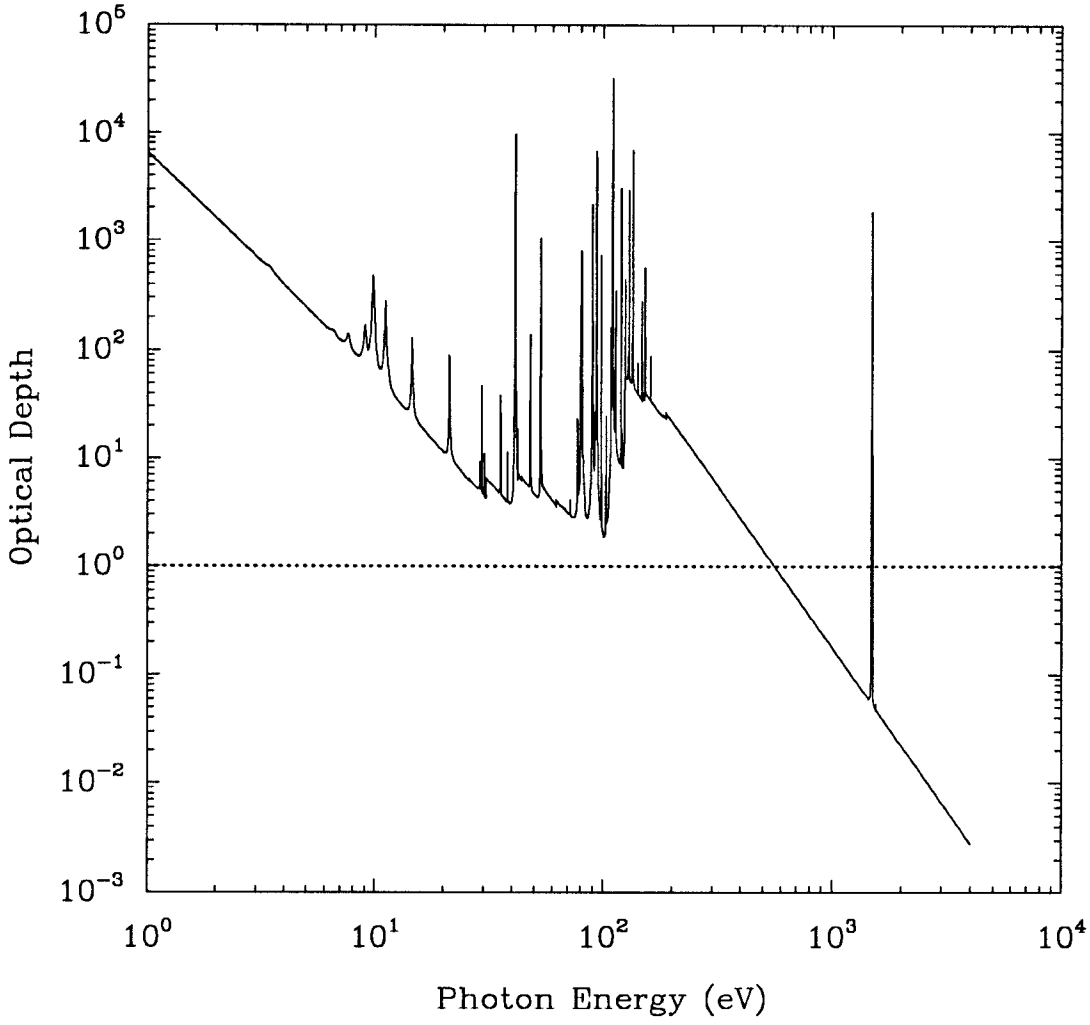

Figure 9. Frequency-dependent optical depths for the case shown in Figure 8. Note the large optical depths for the K_α lines near 1.5 keV.

The ionization indices refer to the ionization stage prior to proton-impact ionization. In the experimental spectrum, the K_α lines of Al I-IV have the largest fluxes. The wavelengths for these ionization stages lie close together because the number of M-shell electrons has little influence on the transition energy. However, as the Al becomes more ionized and the number of L-shell electrons decreases, the K_α lines are noticeably blue-shifted. Ionization stages up to Al IX are clearly seen in the experimental spectrum.

The calculated K_α line positions and relative intensities of the Al I-IV and Al V in Figure 10 agree quite well with the experimental spectrum. This suggests that the portion of the plasma most readily seen by the detector was at a temperature of about 10 eV or below for a majority of time during the experiment. At 10 eV, however, the plasma is too cold to produce K_α line radiation from the higher ionization stages.

Figure 11 shows the K_α spectrum from an Al plasma at 40 eV, $n = 10^{-2}\ n_0$, and $L_0 = 10\ \mu$m. In this case, K_α lines from Al VIII and Al IX have the highest intensities. The calculated wavelengths of the K_α lines line up quite well with the peaks in the experimental spectrum. On the other hand, the relative strengths of the lines are not consistent with the time-integrated spectrum. This indicates that either: (1) the plasma spent a relatively short period of time at these temperatures, or (2) the K_α lines from the higher ionization stages originate in a hotter region of the plasma, and these K_α lines are attenuated by cooler material that resides between the detector and the hot plasma. In this case, the attenuation would be primarily due to L-shell photoabsorption.

The influence of opacity effects on the radiation escaping the plasma is very significant. This is seen in Figure 12, where the K_α line fluxes from a $T = 40$ eV, $n = 10^{-2}\ n_0$, $L =$ 1 mm Al plasma are plotted for two cases. The dotted curve is from a calculation in which attenuation effects were ignored; that is, the plasma was assumed to be optically thin. The solid curve was obtained from calculations in which opacity effects were fully accounted for. Note that the fluxes in the optically thin case are typically 3 orders of magnitude higher than in the optically thick case. It is also seen that the relative fluxes of 2 lines can be significantly influenced by opacity effects. For instance, the Al VIII line at 8.04 Å is about a factor of 5 higher than the Al IX line at 7.98 Å in the optically thin case. However, when opacity effects are included, the lines have peak fluxes that are nearly equal. This clearly demonstrates the importance of transport effects in this spectral region.

It is also of interest to know the location at which the K_α photons originate. Photons at the cores of optically thick lines originate near the "edge" of the plasma; that is, where the line center optical depth becomes small. On the other hand, photons from optically thin lines and those from the wings of optically thick lines can originate deep within the plasma and still be detected. This is shown in Figure 13, where the differential emission flux ($= \partial F(r,\nu)/\partial r$) is plotted as a function of frequency and position at which the photons originate. Note that the position axis is on a logarithmic scale and that the detector is at

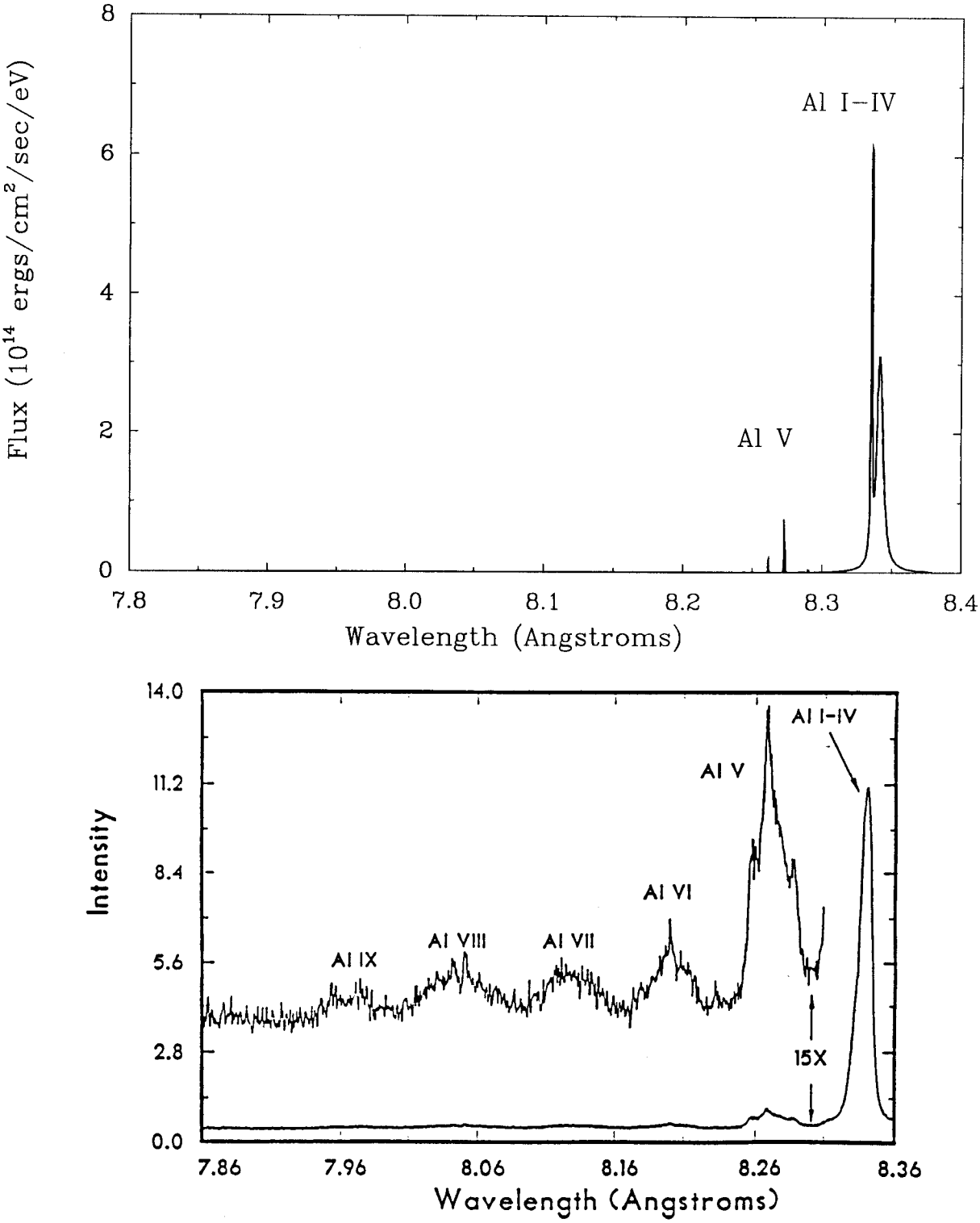

Figure 10. (Top) Calculated K_α line spectrum from an Al plasma at $T = 10$ eV, $n = 10^{-1}\ n_0$, and $L = 0.1$ mm being heated by a 5 MeV, 5 TW/cm^2 proton beam. (Bottom) Experimental time integrated spectrum from Bailey *et al.* (1990).

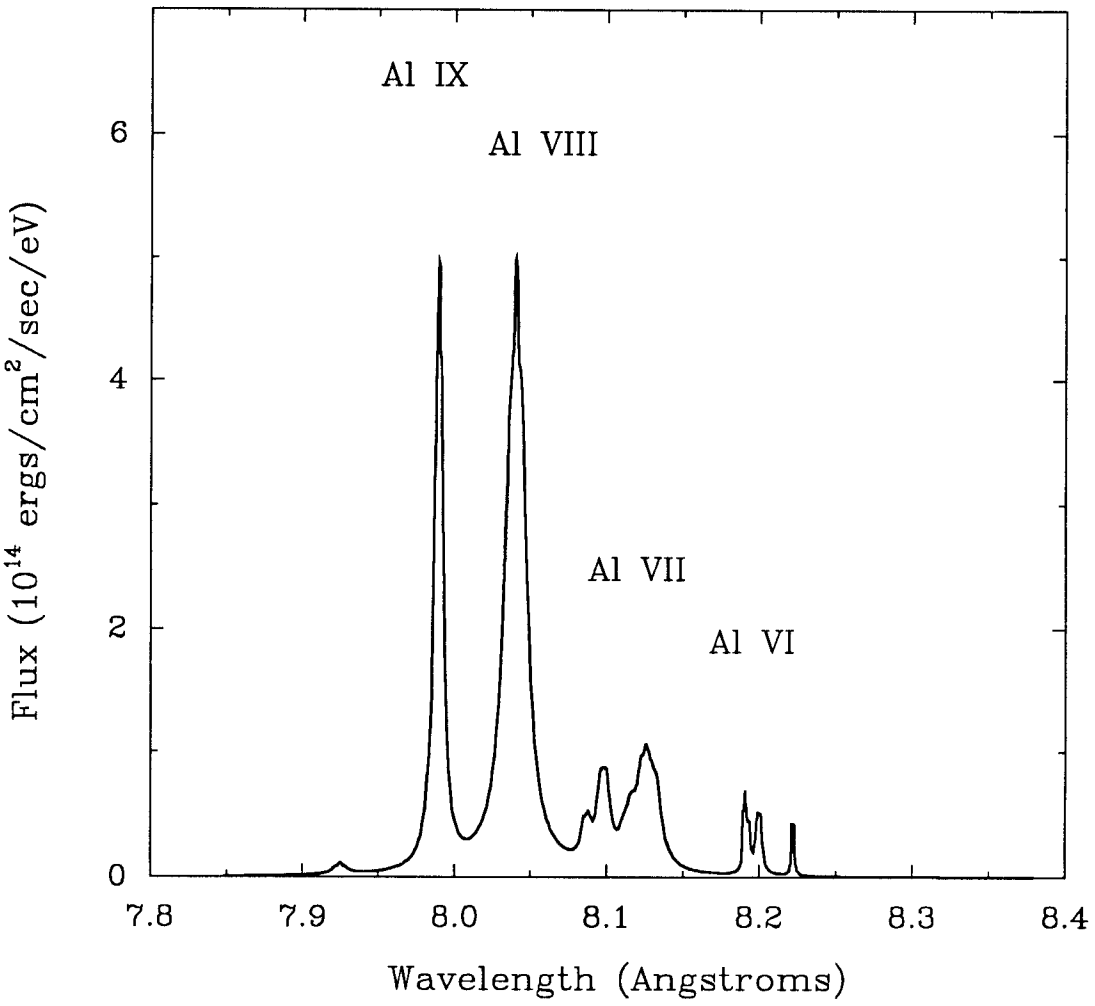

Figure 11. Calculated K_α line spectrum from an Al plasma at $T = 40$ eV, $n = 10^{-2}\ n_0$, and $L = 1.0$ mm being heated by a 5 MeV, 5 TW/cm^2 proton beam.

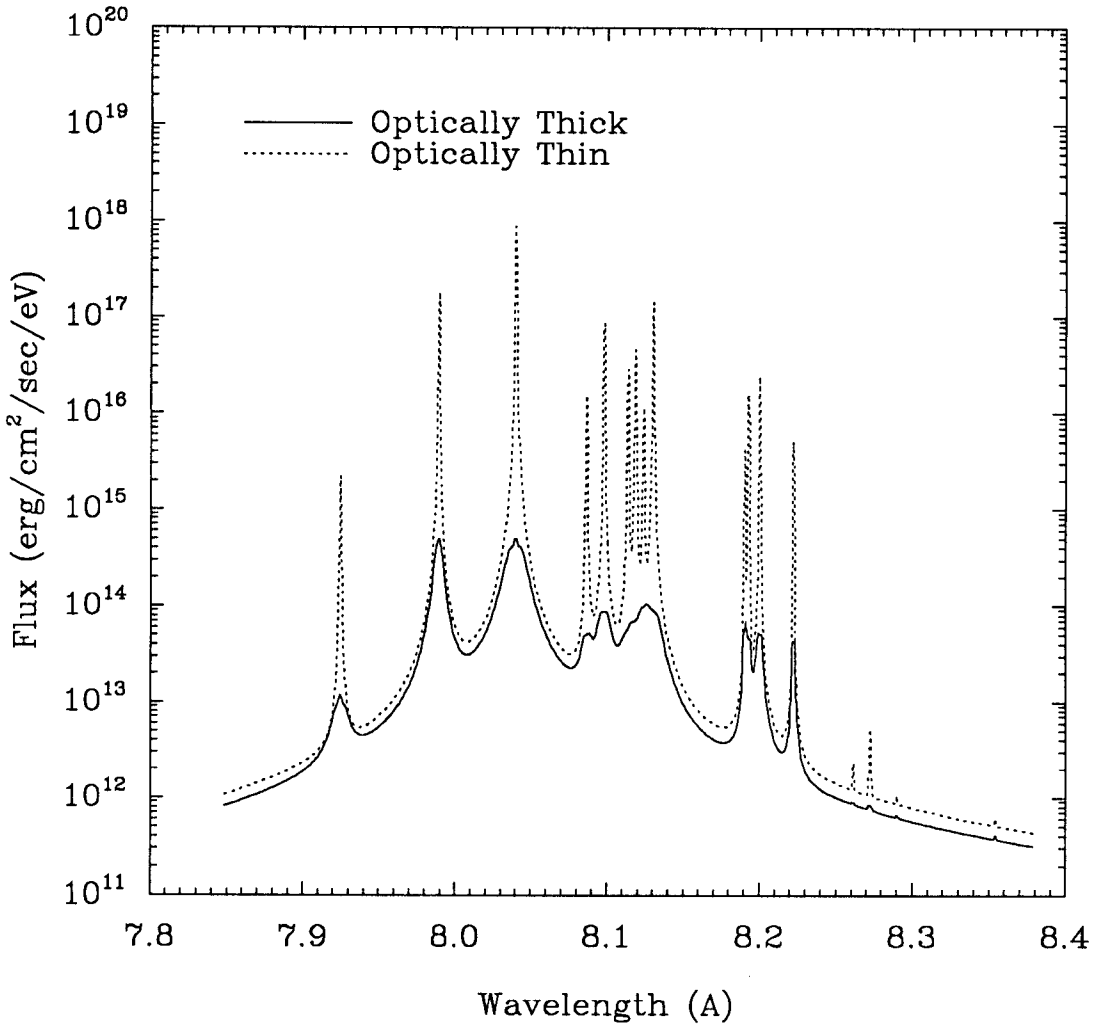

Figure 12. Comparison of K_α spectral fluxes calculated for optically thick (solid curve) and optically thin (dotted curve) Al plasmas. In each case, $T = 40$ eV, $n = 10^{-2}\ n_0$, and $L = 1$ mm.

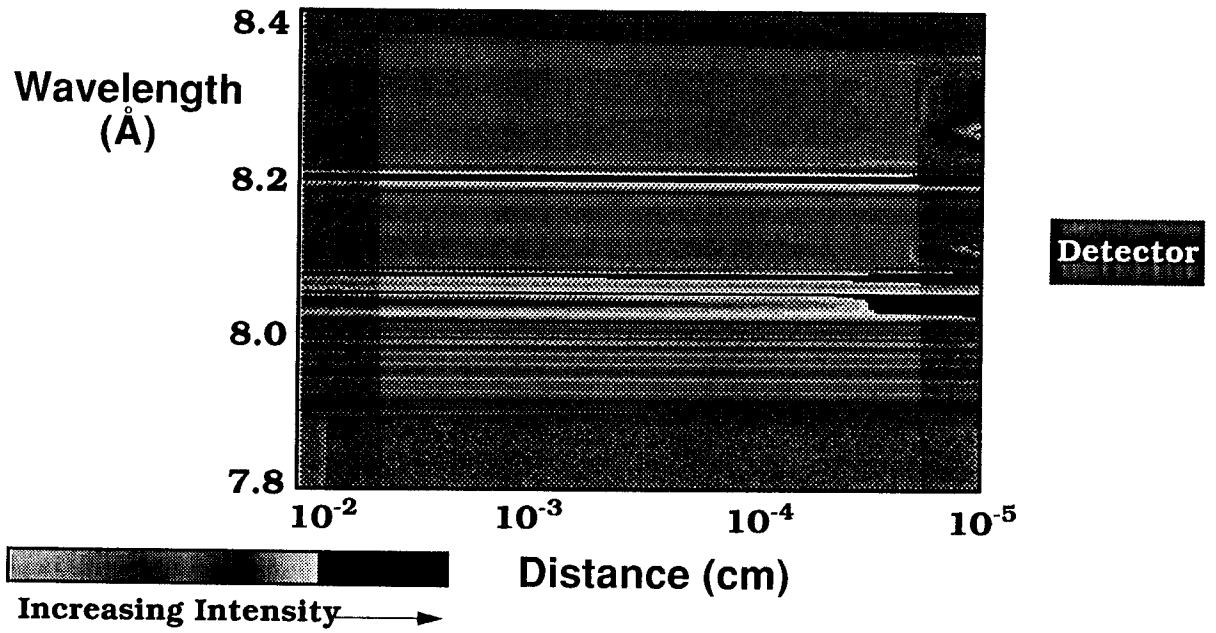

Figure 13. Contribution to the K_α spectral flux seen by a detector as a function of position in the plasma. The areas near the boundary with large intensity gradients indicate that the radiation seen by the detector at those wavelengths originates very close to the boundary. Note that the distance scale is logarithmic.

the right. The relatively dark regions are the regions with the largest fluxes. The way to interpret this plot is to look at the gradients in the differential flux at a given wavelength (in the horizontal direction). At wavelengths where there are significant gradients, such as near 8.05 and 8.20 Å, the flux seen by the detector is due to photons originating very close to the edge of the plasma. At wavelengths where there are no noticeable gradients, the plasma is optically thin and behaves like a volume emitter.

Clearly, ion beam-induced transitions offer many possibilities for deducing plasma conditions in target experiments. Experimental spectra in conjunction with a judicious mix of hydrodynamics simulations and non-LTE radiative transfer calculations can lead to an improved understanding of beam-plasma interaction physics.

4. Summary

We have calculated radiation spectra for ion beam-heated Al plasmas with temperatures $\sim$ 5 eV to 50 eV and ion densities $\sim 10^{-2}$ to 10^{-1} n_0. The dependence of the emission spectrum on the plasma temperature and thickness was studied. It was shown how the bulk of the emergent flux evolves toward a blackbody spectrum as the original foil (target) thickness increases. K_α line spectral fluxes were computed for moderately ionized Al plasmas. The self-attenuation of the K_α line radiation was found to have a significant effect on the emergent flux. In regards to the transition energies and relative intensities, good general agreement was found between our numerical simulations and the experimental K_α spectrum obtained at Sandia National Laboratories on PBFA II. Our calculations show that K_α satellite line spectra present good opportunities for diagnosing temperatures in ion beam-heated plasmas.

Acknowledgements

The authors gratefully acknowledge support from Kernforschungszentrum Karlsruhe (KfK) through Fusion Power Associates. P. Wang has also been supported in part by Sandia National Laboratories. Computing support was provided in part by the U. S. National Science Foundation through the San Diego Supercomputing Center.

References

Apruzese, J. P. 1981, *J.Q.S.R.T.* **25**, 419.

Apruzese, J. P., Davis, J., Duston, D., and Clark, R. W. 1984, *Phys. Rev. A* **29**, 246.

Apruzese, J. P., Davis, J., Duston, D., and Whitney, K. G. 1980, *J.Q.S.R.T.* **23**, 479.

Bailey, J., Carlson, A. L., Chandler, G., Derson, M. S., Dukart, R. J., Hammel, B. A., Johnson, D. J., Lockner, T. R., Maenshen, J., McGuire, E. J., Melhorn, T. A., Nelson, W. E., Ruggles, L. E., Stygar, W. A., and Wenger, D. F. 1991, *Lasers Part. Beams*, **8**, 555.

Bauer, W., Bluhm, H., and Goel, B. 1988, Kernforschungszentrum Karlsruhe Report 14-04-02P-16A, Karlsruhe, Germany.

Burgess, A., and Summer, H. P. 1976, *Mon. Not. R. Astr. Soc.* **174**, 345.

Chenais-Popovics, C., Fievet, C., Geindre, J. P., Gauthier, J. C., Luc Koenig, E., Wyart, J. F., Pepin, H., and Chaker, M. 1989, *Phys. Rev. A.* **40**, 3194.

Clark, R. W., Davis, J., and Cochran, F. L. 1986, *Phys. Fluids* **29**, 1971.

Duston, D., Clark, R. W., Davis, J., and Apruzese, J. P. 1983, *Phys. Rev. A* **27**, 1441.

Duston, D., and Davis, J. 1981, *Phys. Rev. A.* **23**, 2602.

Froese Fischer, C. 1978, *Comp. Phys. Commun.* **14**, 145.

Hoffmann, D. D. H., Hofmann, I., and Meyer-ter-Vehn, J. 1990, Gesellschaft für Schwerionenforschung Report GSI-90-15, Darmstadt, Germany.

Khan, J. M., Potter, D. L., and Worley, R. D. 1965, *Phys. Rev.* **139**, A1735.

MacFarlane, J. J., Wang, P., and Henderson, D. L. 1991, University of Wisconsin Fusion Technology Institute Report UWFDM-847 and Fusion Power Associates Report FPA-91-1, Madison, WI.

MacFarlane, J. J., Wang, P., and Moses, G. A. 1990a, University of Wisconsin Fusion Technology Institute Report UWFDM-822 and Fusion Power Associates Report FPA-90-1, Madison, WI.

MacFarlane, J. J., Wang, P., and Moses, G. A. 1990b, *Lasers Part. Beams*, **8**, 729.

Merzbacher, E., and Lewis, H. W. 1958, in Handbuch der Physik, Vol. 34, ed. S. Flugge (Springer-Verlag, Berlin).

Meyer-ter-Vehn, J., and Witkowski, S. 1990, *Phys. Fluids B* **2**, 1313.

Nardi, E., and Zinamon, Z. 1981, *J. Appl. Phys.* **52**, 7025.

Post, D. E., Jensen, R. V., Tarter, C. B., Grasberger, W. H., and Lokke, W. A. 1977, *At. Data Nucl. Data Tables* **20**, 397.

Rogerson, J. E., Clark, R. W., and Davis, J. 1985, *Phys. Rev. A.* **31**, 3323.

Sobelman, I. I., Vainshtein, L. A., and Yukov, E. A. 1981, Excitation of Atoms and Broadening of Spectral Lines (Springer-Verlag, New York).

Wang, P. 1991, Ph.D. Dissertation, Dept. of Nuclear Engineering and Engineering Physics, University of Wisconsin, in preparation.